energies

MDPI

Article

A Polynomial Synthesis Approach to Design and Control an LCL-Filter-Based PWM Rectifier with Extended Functions Validated by SIL Simulations

Rosa Iris Viera Díaz, Ciro Nuñez *, Nancy Visairo Cruz and Juan Segundo Ramírez

Facultad de Ingeniería, Universidad Autónoma de San Luis Potosí, San Luis Potosí 78290, Mexico; rosair.viera@gmail.com (R.I.V.D.); nvisairoc@uaslp.mx (N.V.C.); juan.segundo@uaslp.mx (J.S.R.)
* Correspondence: calberto@uaslp.mx; Tel.: +52-444-826-2300 (ext. 6264)

Abstract: Controlling a PWM rectifier can be challenging due to the bilinear nature of its averaged model. This paper introduces the use of the Butterworth approach to design and control an LCL-filter-based PWM rectifier with power quality functions. By leveraging the linear part of the system, this approach reduces the number of variables involved in the control scheme. The rectifier is designed and controlled in a concatenated manner to ensure proper performance even during demanding power-quality events. The uniqueness of this approach lies in the fact that a fourth-order model can be regulated by using solely three-state variables and linear techniques founded on Butterworth polynomial synthesis. This approach differs from previous methods in that it does not employ nonlinear controllers, *dq* transformations, or double control loops. Hence, this divergent approach contributes to the simplification of power converter design and control through the application of the same polynomial synthesis, besides enhancing system operation in demanding scenarios. Extensive SIL simulations of a 1 kW, 220 Vrms PWM rectifier using the OPAL-RT-1400 platform were conducted to demonstrate the feasibility of the proposed controller. The selected tests reveal the validity of this proposal even when the PWM rectifier faces multiple power quality events simultaneously.

Keywords: harmonic current compensation; LCL filter; PWM rectifier; state feedback control

Citation: Viera Díaz, R.I.; Nuñez, C.; Visairo Cruz, N.; Segundo Ramírez, J. A Polynomial Synthesis Approach to Design and Control an LCL-Filter-Based PWM Rectifier with Extended Functions Validated by SIL Simulations. *Energies* **2023**, *16*, 7382. https://doi.org/10.3390/en16217382

Academic Editor: Yu Zhang

Received: 6 October 2023
Revised: 14 October 2023
Accepted: 24 October 2023
Published: 31 October 2023

1. Introduction

Power conversion has a long history of using front-end rectifiers that rely on active components, even when vacuum valves were considered cutting-edge technology [1]. Over time, these rectifiers have evolved to become PWM rectifiers, which are now utilized for a range of control objectives, including power factor correction, harmonic compensation, AC voltage unbalanced operation, and so on [2–5].

Multiple references exist to support these developments. Before such an amount of control objectives, naturally, the applications grew in variety. For instance, PWM rectifiers for motor drives were investigated when semiconductor technology advanced in terms of capabilities [6]. Also, alongside the use of a PWM rectifier, other capabilities related to power quality were explored such as voltage sag ride through [7], harmonic compensation [3], power factor compensation [8], and even fault-tolerant operation [9].

Groundbreaking applications are also related to PWM rectifiers because of their multiple functionalities. For example, the doubly-fed induction generator (DFIG) wind technology uses a PWM rectifier in its operative blocks to ensure that the DC bus remains stable, which is crucial for the stability of the entire power system [10]. This is also true for photovoltaic (PV) systems that integrate large battery energy storage systems into the grid [11]. In these cases, the PWM rectifier transfers grid energy to the battery with high quality standards. The same applies to electric vehicle (EV) applications, where a PWM rectifier is used, as referenced in [12,13].

The previous discussion is interesting from the standpoint of power conversion and its applications. However, as previously explained, the automatic control component is necessary to successfully achieve these objectives. For the inherently bilinear model of the PWM rectifier, some researchers propose nonlinear control approaches to provide the converter with desired capabilities, but they can be challenging to implement in practical cases [2,14,15]. Those approaches are attractive because nonlinear controllers permit the system performance around the complete range of operations. However, understanding the nonlinear philosophy can be confusing for practical engineers, and their incorporation as a helpful tool is a pendent assignment for future engineers.

Addressing the control detail, multiple references report the non-minimal phase behavior of boost topologies such as the PWM rectifier [16,17], and due to that, it is natural to find double loop controllers—DC voltage and AC current—either for linear or nonlinear approaches, increasing the processing amount of signals. From a linear standpoint, the *dq* transformation and linearization are commonly used, since the tracking control problem can be changed into a regulation problem [8,18,19]. The price to be paid is that the inverse transformation should be made for controlling the system in the time domain.

This paper presents a different approach for designing and controlling a bi-phase PWM rectifier with LCL filter input. The proposed approach has a significant conceptual advantage over other approaches in that it uses only the linear part of the averaged model to design the LCL filter and tune the controller by concatenating the same polynomial synthesis. On the other hand, most of the existing works use *dq* transformations, double control loops, or nonlinear controllers, as can be seen in [20]. In straightforward terms, this paper formulates that a fourth-order system is controlled by using the third-order linear part. Another advantage of this approach is that it can be extended to both other filter order and three-phase systems. The design and control tuning are concatenated in a polynomial approach based on the Butterworth polynomial. In order to validate the proposed method, software-in-the-loop (SIL) simulations of a 1 kW, 220 Vrms PWM rectifier, applying a sinusoidal PWM technique (SPWM), are presented by using a real-time OPAL RT-1400 setup through an OP4510 simulation target as shown in Figure 1.

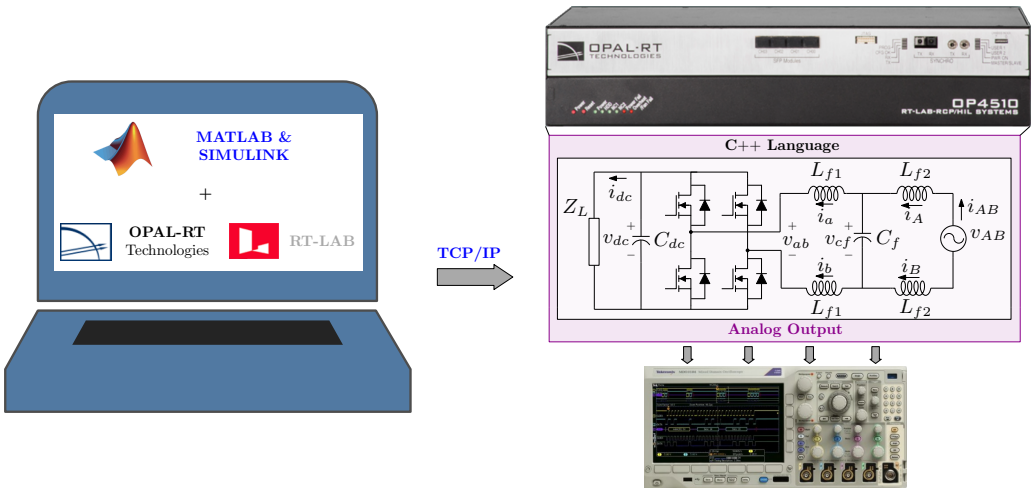

Figure 1. SIL simulation setup for testing the PWM rectifier with LCL filter.

The organization of the article is as follows: Section 2 presents the electrical specifications to be accomplished by the bi-phase PWM rectifier alongside its modeling and the LCL filter design. In Section 3, the control tuning is developed and explained. Section 4 is devoted to presenting the test demonstrations with SIL simulations by using OPAL RT-1400. Section 5 is dedicated to discussing and concluding the findings and achievements of the research.

2. LCL-Filter-Based PWM Rectifier

2.1. Parameters and Capabilities

In this paper, a challenging electrical performance profile is presented to demonstrate the wide range of functionality of the proposed control scheme. Table 1 reports the steady-state electrical parameters and the extended functions to be tested, while Figure 1 illustrates the SIL simulation used for testing the PWM rectifier. It can be noticed that this proposal includes an LCL filter interconnected between the grid and the power converter, where v_{AB} is the grid voltage; v_{ab} is the PWM voltage; v_{cf} is the voltage of the capacitor C_f; i_a, i_b, and i_A, i_B are the currents through the inductors L_{f1} and L_{f2}, respectively; i_{AB} is the grid current; v_{dc} is the DC bus voltage; C_{dc} is the DC capacitor; and Z_L is any load—depending on the application—at the DC side.

Table 1. Steady state and extended functions for a 1 kW PWM rectifier.

Parameter or Condition	Symbol	Value
Nominal active power.	P_{rect}	1 kW
Grid voltage.	V_{AB}	220 V_{rms} ± 10%
Power factor.	PF	≈1
Grid current total harmonic distorsion.	THD_{iAB}	≤5% (at full load)
DC bus voltage reference.	V_{dc}	420 V ± 2.4%
Grid voltage sag ride-through capability.		yes
Harmonic current compensation capability.		yes
Dynamical DC load and voltage sag ride-through capability simultaneously.		yes
±10% DC bus voltage variation capability.		yes
Dynamical DC load, voltage sag ride-through and harmonic current compensation simultaneously.		yes

2.2. Modeling

To formulate the proposed concept, the modeling of the PWM rectifier is addressed with the following considerations:

- The PWM rectifier is modeled in the time domain considering the average model. This modeling is justified because the switching frequency is high enough with respect to the grid's fundamental frequency.
- The components are considered ideal. This consideration is justified because the effect of an integrator that will be introduced into the closed-loop controller has the capability of robustness against constant parameter variations, such as parasitic parameters.

Once the assumptions have been established, the average model of the PWM rectifier can be written as:

$$\begin{bmatrix} \dot{x_1} \\ \dot{x_2} \\ \dot{x_3} \\ \dot{x_4} \end{bmatrix} = \begin{bmatrix} 0 & 0 & \frac{1}{3L_{f1}} & \frac{-v_{ab}}{3L_{f1}} \\ 0 & 0 & \frac{-1}{3L_{f2}} & 0 \\ \frac{-3}{C_f} & \frac{3}{C_f} & 0 & 0 \\ \frac{v_{ab}}{C_{dc}} & 0 & 0 & \frac{1}{Z_L C_{dc}} \end{bmatrix} \begin{bmatrix} x_1 \\ x_2 \\ x_3 \\ x_4 \end{bmatrix} + \begin{bmatrix} 0 \\ \frac{v_{AB}}{3L_{f2}} \\ 0 \\ 0 \end{bmatrix}, \tag{1}$$

where

$$\begin{aligned} \mathbf{x} &= \begin{bmatrix} i_{ab} \; i_{AB} \; v_{cf} \; v_{dc} \end{bmatrix}^T, \\ i_{ab} &= \frac{1}{3}(i_a - i_b), \\ i_{AB} &= \frac{1}{3}(i_A - i_B). \end{aligned} \tag{2}$$

The fourth column and the fourth row of the state matrix of (1) show the bilinear nature of the average model, since the PWM signal v_{ab} appears, multiplying the state variables x_4 and x_1, respectively. This feature will be explored later to formulate the proposed concept.

2.3. LCL Filter Design

For the LCL filter design, the handbook of filter synthesis is used [21]. Although its main focus is on communication applications, the mathematical principles are useful for power conversion. Hence, Figure 2 illustrates the design of a third order filter.

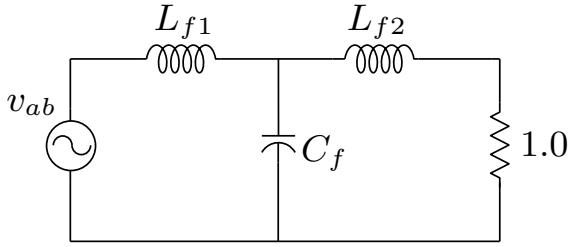

Figure 2. LCL filter of [21] using Butterworth concept.

The small signal model of the PWM rectifier in Figure 1 is presented in Figure 3. This last figure is used to formulate—by using a comparison between Figures 2 and 3—the concept of the filter design and the control tuning. Note that, in Figure 3, the left side is the circuit part where the bilinearity of (1) originates.

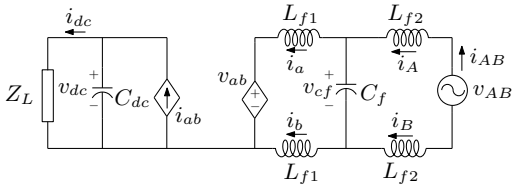

Figure 3. Small signal model of the PWM rectifier.

For the LCL filter design, consider the following step-by-step procedure:

1. Select the filter order n. In this case, $n = 3$.
2. From the power specification of the PWM rectifier on the DC side, consider that the AC power is the same, i.e., $\eta = 1$. For practical design, η can be selected as lower than one.
3. Calculate a "virtual" resistance R_{virt}, whose value shall represent the AC power P_{AB} needed to cover the DC power requirements, as shown in Figure 4.
4. Select the switching frequency f_{sw} and the cut frequency $w_{c,virt}$, where $f_{sw} = m_f f_1$, with the frequency modulation index $m_f = 155$, the fundamental frequency $f_1 = 60$ Hz, and $w_{c,virt}$ is selected one decade lower than f_{sw}; thus, $w_{c,virt} = (0.1)2\pi f_{sw} = 0.1 w_{sw}$. Note that $w_{c,virt}$ can be obtained for a desired attenuation of the most relevant harmonics of v_{ab} according to the needed specification.
5. Calculate the values of the LCL filter according to Zverev method [21]: (i) For a third order filter, the normalized values are

$$L_{f1,n} = 1.5/3, \quad L_{f2,n} = 0.5/3, \quad C_{f,n} = 3 \times 1.3333; \tag{3}$$

(ii) Then, denormalizing

$$L_{f1} = \frac{R_{virt}\, L_{f1,n}}{w_{c,virt}}, \quad L_{f2} = \frac{R_{virt}\, L_{f2,n}}{w_{c,virt}}, \quad C_f = \frac{C_{f,n}}{R_{virt}\, w_{c,virt}}. \tag{4}$$

Applying the above procedure, it is obtained that

$$R_{virt} = \frac{V_{AB}^2}{P_{AB}} = \frac{220^2}{1000} = 48.4\ \Omega, \qquad w_{c,virt} = 5.84\ \text{krad/s}, \tag{5}$$

$$L_{f1} = 4.14\ \text{mH}, \qquad L_{f2} = 1.38\ \text{mH}, \qquad C_f = 14.14\ \mu\text{F}. \tag{6}$$

The flow chart shown in Figure 5 summarizes the step-by-step LCL filter design procedure.

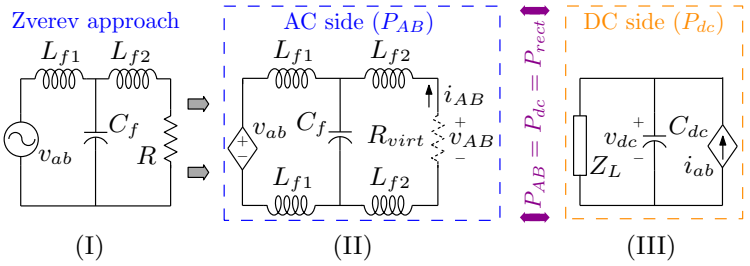

Figure 4. Filter design graphical formulation based on the Zverev method.

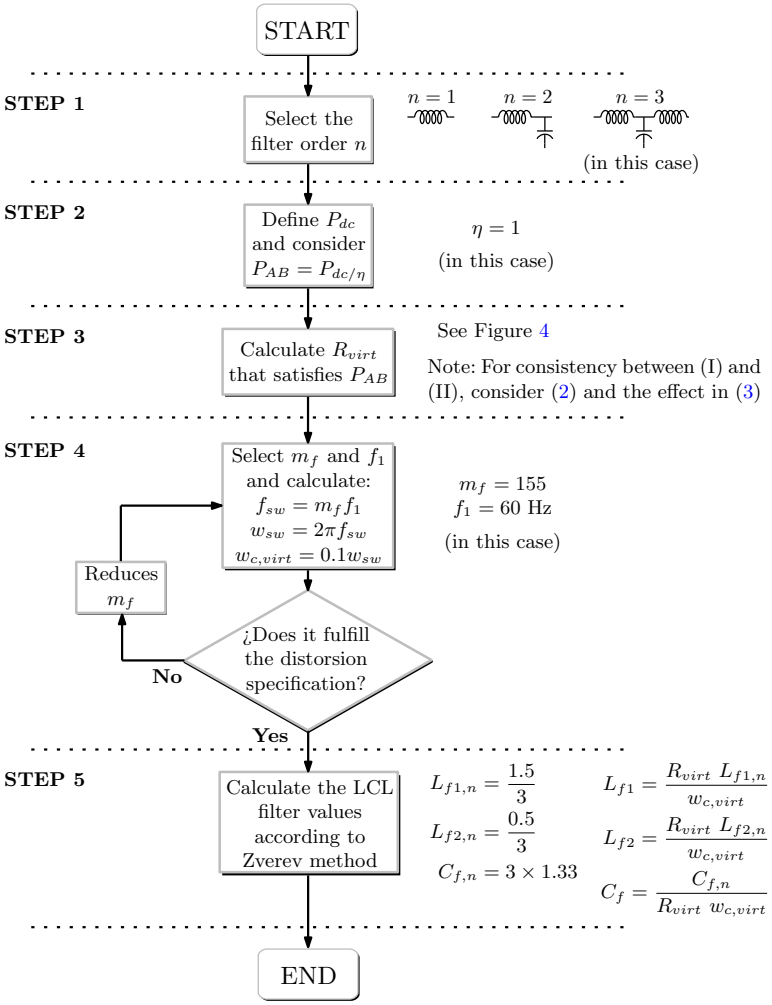

Figure 5. Step-by-step LCL filter design procedure based on the Zverev method.

3. Control System Design

Linear controllers have an important role in the industrial environment due to their easy understandability, low complexity design, and good performance. Keeping this in mind, a linear control for the PWM rectifier is proposed, which can be more easily accepted to be implemented in industrial boards, whether digital or analog.

For control purposes, the following considerations are stated:

- As the LCL filter was designed to cope with the DC power requirements, a linear controller is proposed just for controlling the power flux through the LCL filter.
- To tune the controller, some rearrangements should be made to (1) as follows:

$$\begin{bmatrix} \dot{x_1} \\ \dot{x_2} \\ \dot{x_3} \end{bmatrix} = \begin{bmatrix} 0 & 0 & \frac{1}{3L_{f1}} \\ 0 & 0 & \frac{-1}{3L_{f2}} \\ \frac{-3}{C_f} & \frac{3}{C_f} & 0 \end{bmatrix} \begin{bmatrix} x_1 \\ x_2 \\ x_3 \end{bmatrix} + \begin{bmatrix} \frac{-x_4}{3L_{f1}} \\ 0 \\ 0 \end{bmatrix} v_{ab} + \begin{bmatrix} 0 \\ \frac{1}{3L_{f2}} \\ 0 \end{bmatrix} v_{AB}, \tag{7}$$

$$\begin{bmatrix} \dot{x_4} \end{bmatrix} = \begin{bmatrix} \frac{v_{ab}}{C_{dc}} & 0 & 0 & \frac{1}{Z_L C_{dc}} \end{bmatrix} \begin{bmatrix} x_1 \\ x_2 \\ x_3 \\ x_4 \end{bmatrix}, \tag{8}$$

where (7) corresponds to the LCL filter with its control signal v_{ab} as shown in Figure 4 (II), and (8) represents the DC bus voltage dynamics, illustrated in Figure 4 (III).

A strong assumption by which to consider (7) as a linear equation is that the state variable x_4 exists as a constant, i.e., $x_4 \approx V_{dc}$. Due to the rectifier's nature, which has AC time-variant voltage and current at the input port—AC grid side—and constant-time average voltage at the output port—DC bus side—the previous assumption is considered valid. The apparent algebraic loop generated by that assumption can be broken if a soft start strategy is applied at the beginning of the rectifier operation at $t = 0$ s followed by a closed-loop operation once $x_4 = V_{dc}$.

Thus, the open-loop linear matrices of the third-order system are:

$$\mathbf{A} = \begin{bmatrix} 0 & 0 & \frac{1}{3L_{f1}} \\ 0 & 0 & \frac{-1}{3L_{f2}} \\ \frac{-3}{C_f} & \frac{3}{C_f} & 0 \end{bmatrix}, \ \mathbf{b_1} = \begin{bmatrix} \frac{-(x_4 = V_{dc})}{3L_{f1}} \\ 0 \\ 0 \end{bmatrix}, \ \mathbf{b_2} = \begin{bmatrix} 0 \\ \frac{1}{3L_{f2}} \\ 0 \end{bmatrix}, \ \mathbf{c} = \begin{bmatrix} 0 & 1 & 0 \end{bmatrix}. \tag{9}$$

Figure 6 shows in red color the open-loop eigenvalues at the imaginary axis, thus the system is undamped, which is undesirable for the PWM rectifier operation. Therefore, in order to achieve a good performance in a closed-loop, a state feedback with an integrator is proposed in this work, as shown in Figure 7.

From Figure 7, the system equations in the closed-loop can be derived as:

$$\begin{aligned} \begin{bmatrix} \dot{\mathbf{x}} \\ \dot{\sigma} \end{bmatrix} &= \begin{bmatrix} \mathbf{A} + \mathbf{b_1 k} & \mathbf{b_1} k_i \\ -\mathbf{c} & 0 \end{bmatrix} \begin{bmatrix} \mathbf{x} \\ \sigma \end{bmatrix} + \begin{bmatrix} 0 \\ 1 \end{bmatrix} x_2^r + \begin{bmatrix} \mathbf{b_2} \\ 0 \end{bmatrix} v_{AB}, \\ &= \hat{\mathbf{A}} \begin{bmatrix} \mathbf{x} \\ \sigma \end{bmatrix} + \begin{bmatrix} 0 \\ 1 \end{bmatrix} x_2^r + \begin{bmatrix} \mathbf{b_2} \\ 0 \end{bmatrix} v_{AB}. \end{aligned} \tag{10}$$

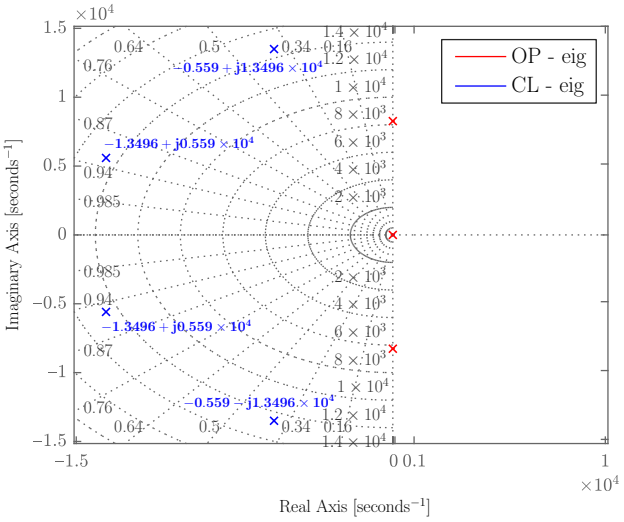

Figure 6. Root locus of the open and closed-loop eigenvalues of the system.

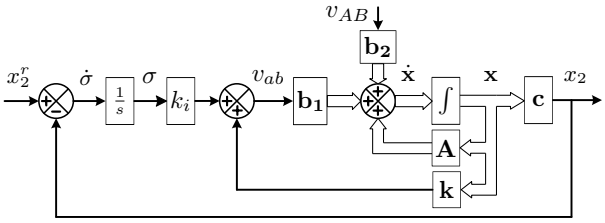

Figure 7. Block diagram of the state feedback with an integrator.

The next step is the control tuning, that is, to select the values of $\mathbf{k}$ and k_i in such a way that the matrix $\hat{\mathbf{A}}$ results in a Hurwitz matrix; nevertheless, there are some restrictions to take into account. Although any value of $\mathbf{k}$ and k_i that fulfills the Hurwitz condition of $\hat{\mathbf{A}}$ is valid, the PWM rectifier has physical limitations to transferring power from the AC to the DC side; hence, the set of possible values of tuning gains is restricted.

Considering the research reported in [22], the boundaries are established for the root locus of the closed-loop eigenvalues. The concept can be observed in Figure 8, where the upper limit is set by the switching frequency w_{sw}. The closed-loop wide band w_{ncl} is proposed as $w_{ncl} = Mw_{c,virt} < w_{sw}$, where M is a positive real number. Note that, in Figure 8, the closed-loop root locus of the fourth order is produced by applying the proposed controller of (10) to the reduced third-order linear model of (7).

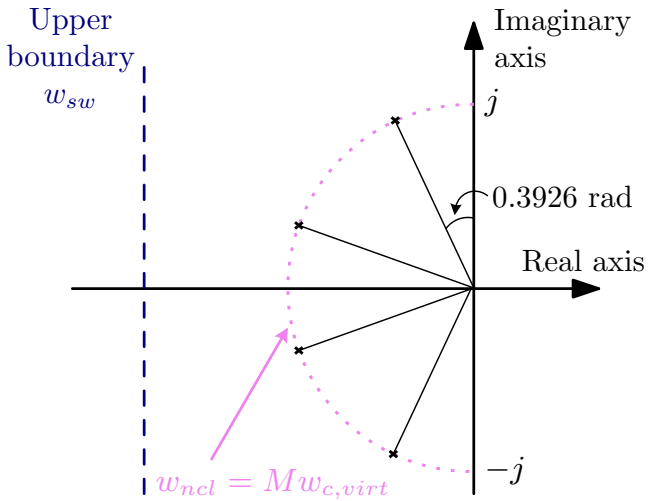

Figure 8. Closed-loop root locus with Butterworth approach.

Proposing $M = 2.5$ and using the Ackerman formula for calculating the controller gains, the results obtained are: $k_1 = -1.129$, $k_2 = -3.574$, $k_3 = 0.092$, and $k_i = 26295$. Figure 6 shows the root locus of the system in open- and closed-loops. As can be seen, the closed-loop eigenvalues increase $M = 2.5$ times $w_{c,virt}$, by the control law $v_{ab} = k_1x_1 + k_2x_2 + k_3x_3 + k_i\sigma$ and $\dot{\sigma} = x_2^r - x_2$.

With this different concept for designing both the LCL filter and the control tuning, the system (1) achieves the desired performance.

4. Software-in-the-Loop Simulation Results of the PWM Rectifier

In engineering, software-in-the-loop simulation integrates compiled production code into a mathematical model simulation. Engineers can use this to develop and test detailed control strategies for large and complex systems in a virtual environment before hardware prototyping. Figure 1 illustrates the SIL setup.

In order to validate the concept, simulation tests are developed in MATLAB & RT-LAB through an OP4510 simulation target based on Opal RT-1400. The PWM rectifier modeled by the system (1) is shown in Figure 9. Additionally, to challenge the control concept, a nonlinear load (NLL) is connected at the point of common coupling (PCC) with the following characteristics:

$$\begin{aligned} i_{nll} = &\frac{I_1}{h_1}\sin(h_1 w_g + \phi_1) + \frac{I_1}{h_3}\sin(h_3 w_g + \phi_3) + \frac{I_1}{h_5}\sin(h_5 w_g + \phi_5) \\ &+ \frac{I_1}{h_7}\sin(h_7 w_g + \phi_7) + \frac{I_1}{h_9}\sin(h_9 w_g + \phi_9) + \frac{I_1}{h_{11}}\sin(h_{11} w_g + \phi_{11}), \end{aligned} \tag{11}$$

where $I_1 = 4$ A is the peak value of the NLL fundamental component, h_j are the harmonics with $j = 1, 3, 5, 7, 9, 11$, and ϕ_j are the shift angles respect to the grid voltage v_{AB} with $\phi_1 = 0°$, $\phi_3 = 38°$, $\phi_5 = 25°$, $\phi_7 = 18°$, $\phi_9 = 15°$, $\phi_{11} = 12°$. According to this harmonic spectrum, the total harmonic distortion (THD) of the NLL current is 42.88%. The aim of the PWM rectifier will be the compensation of harmonics from the third to the eleventh.

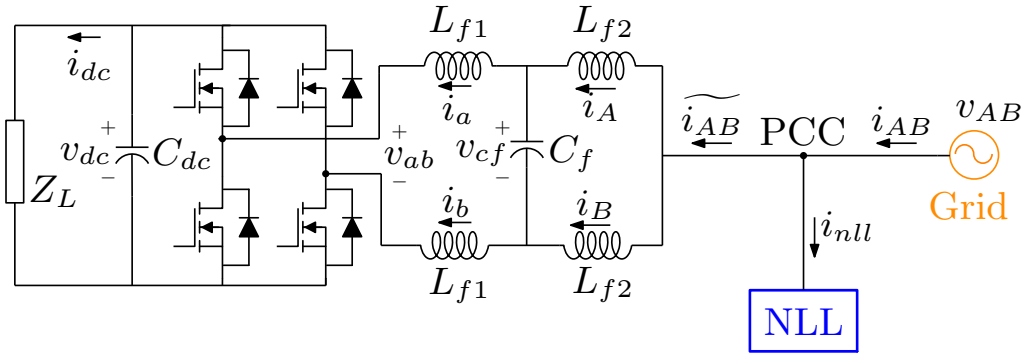

Figure 9. PWM rectifier representation using LCL filter and compensating the harmonic current of a nonlinear load connected at the PCC.

Next, the behavior of the rectifier at different operating points is presented by using the parameters from Table 2. Note that, as long as the NLL is disconnected, $\widetilde{i_{AB}} = i_{AB}$ holds.

Table 2. Parameters of SIL simulations.

Parameter	Symbol	Value
Nominal active power	P_{rect}	1 kW
Grid voltage	V_{AB}	220 V_{rms}
DC bus voltage reference	V_{dc}	420 V
Rectifier switching frequency	f_{rect}	9.3 kHz
Grid frequency	f_g, w_g	60 Hz, 377 rad/s
DC-link capacitor	C_{dc}	5000 µF
Rectifier side inductance	L_{f1}	4.14 mH
Grid side inductance	L_{f2}	1.38 mH
Capacitor of the LCL filter	C_f	14.14 µF
DC equivalent load resistance	Z_L	176.4 Ω
Controller gains	k_1, k_2, k_3, k_i	−1.13, −3.57, 0.09, 26,295
Time step	t_s	10 µs
Active power of the NLL	P_{nll}	622.22 W (62% P_{rect})
THD current of the NLL	THD_{nll}	42.88%

4.1. Steady-State Performance

Figure 10 illustrates the steady-state performance of the PWM rectifier, operating at nominal parameters, without connecting the NLL. The four state variables of (1) are presented in Figure 10a, and it can be seen that the grid current i_{AB} has a low harmonic content (as shown in Figure 10d, resulting in a $\text{THD}_{iAB} < 1\%$, fulfilling the requirements of the IEEE standard [23]. A near unity power factor can be observed from Figure 10c, as well as that the value of the DC current i_{dc} corresponds to the DC load resistance $Z_L = 176.4\ \Omega$. From the PWM voltage v_{ab} shown in Figure 10b, the amplitude of the modulating signal can be calculated as $|u_{ab}| = |v_{ab}|/V_{dc} = 0.74$.

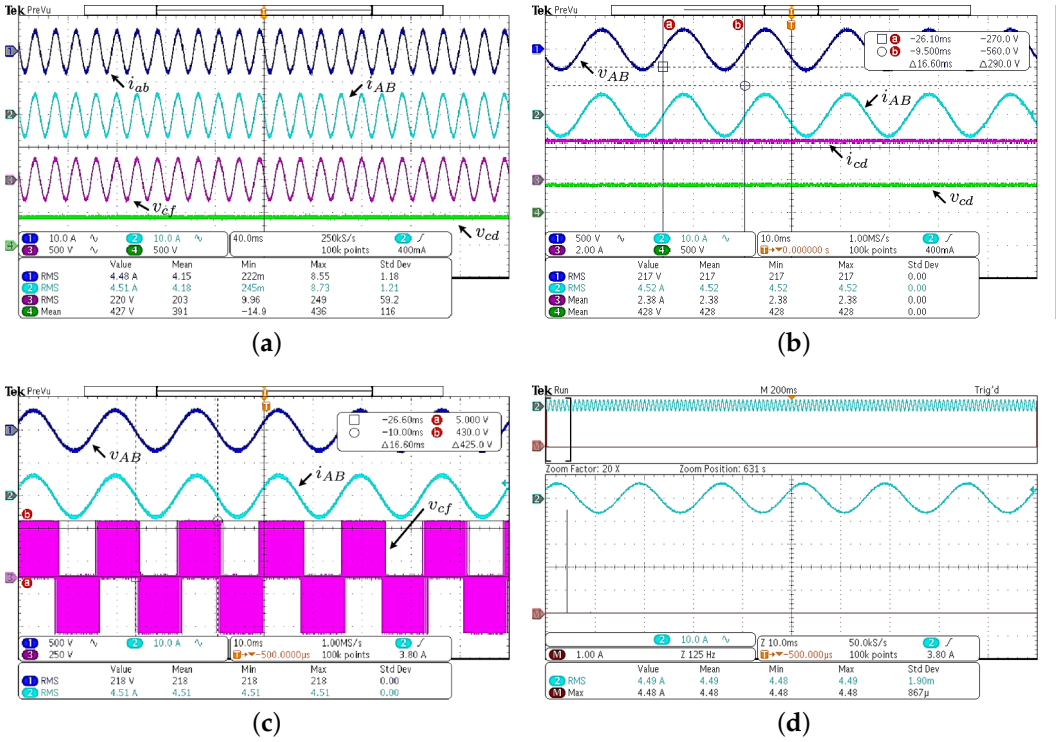

Figure 10. Performance of the PWM rectifier at steady state. (**a**) i_{ab}, i_{AB}, v_{cf} and v_{dc}. (**b**) v_{AB}, i_{AB} and v_{ab}. (**c**) v_{AB}, i_{AB}, i_{dc} and v_{dc}. (**d**) Harmonic spectrum of i_{AB}.

These results reveal the capability of regulating the state variable x_4 by applying the proposed control scheme.

4.2. Grid Voltage Sags without DC Load Variation

For stressing the control scheme facing hard operative conditions, Figure 11 shows the operation of the rectifier when a grid voltage sag occurs periodically. Although periodical sags are unusual, this test reveals the robustness and capabilities of controlling the system with only the third-order linear part of the PWM rectifier. The voltage v_{AB} decreases its nominal value by 25% (until 165 Vrms) while the DC load remains constant. The sag repeats every 1 s. In order to maintain the power balance, the grid current increases its peak value from 6.43 to 8.57 A, and the DC voltage remains regulated.

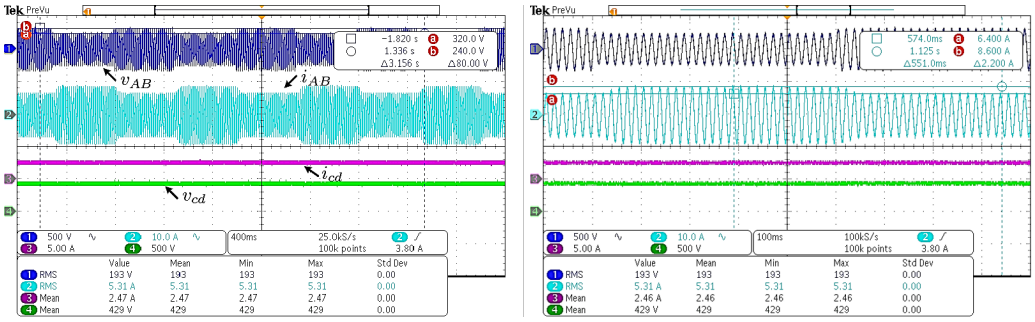

(**a**) (**b**)

Figure 11. Performance of the PWM rectifier under grid voltage sags. (**a**) v_{AB}, i_{AB}, i_{dc} and v_{dc}. (**b**) Zoom in of signals.

4.3. Grid Voltage Sags and Dynamic DC Load Simultaneously

In Figure 12, the DC load changes while grid voltage sags occur with the same aforementioned magnitude. The voltage v_{AB} decreases every 1 s, but simultaneously Z_L is modified with a frequency of 1 kHz. The load changes from 352.8 Ω (corresponding to 500 W) to 117.6 Ω (for 1500 W, representing a 50% of overload), and viceversa; thus, the current i_{dc} switches between 1.22 A and 3.66 A. This result is relevant since it demonstrates the ability to regulate DC voltage even when the PWM rectifier operates outside the nominal operation point.

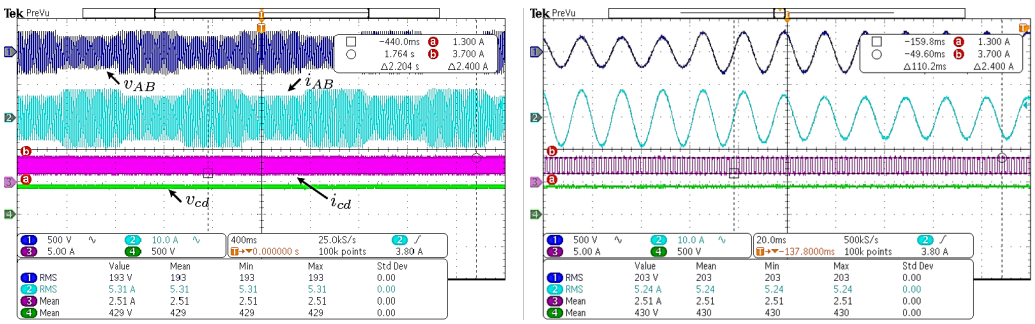

(**a**) (**b**)

Figure 12. Performance of the PWM rectifier under grid voltage sags and load changes. (**a**) v_{AB}, i_{AB}, i_{dc} and v_{dc}. (**b**) Zoom in of signals.

4.4. DC Voltage Reference Changes

Figure 13 illustrates the behavior of the system under different DC voltage reference variations. Figure 13a,b show how the voltage v_{dc} follows its reference V_{dc} when the last one decreases from its nominal value of 420 V to 378 V (−10% of V_{dc}) or increases from 420 V to 462 V (+10% of V_{dc}), respectively. Also, in Figure 13c,d, it can be seen that the system performs well even when V_{dc} changes from +10% to −10% of V_{dc} and vice versa. Since the reference of the current i_{AB} is directly proportional to V_{dc}, its peak value modifies as V_{dc} varies. This is also applied to the current i_{dc}, as long as the DC load remains constant. Note that the voltage v_{dc} takes approximately 1.5 s to reach its reference.

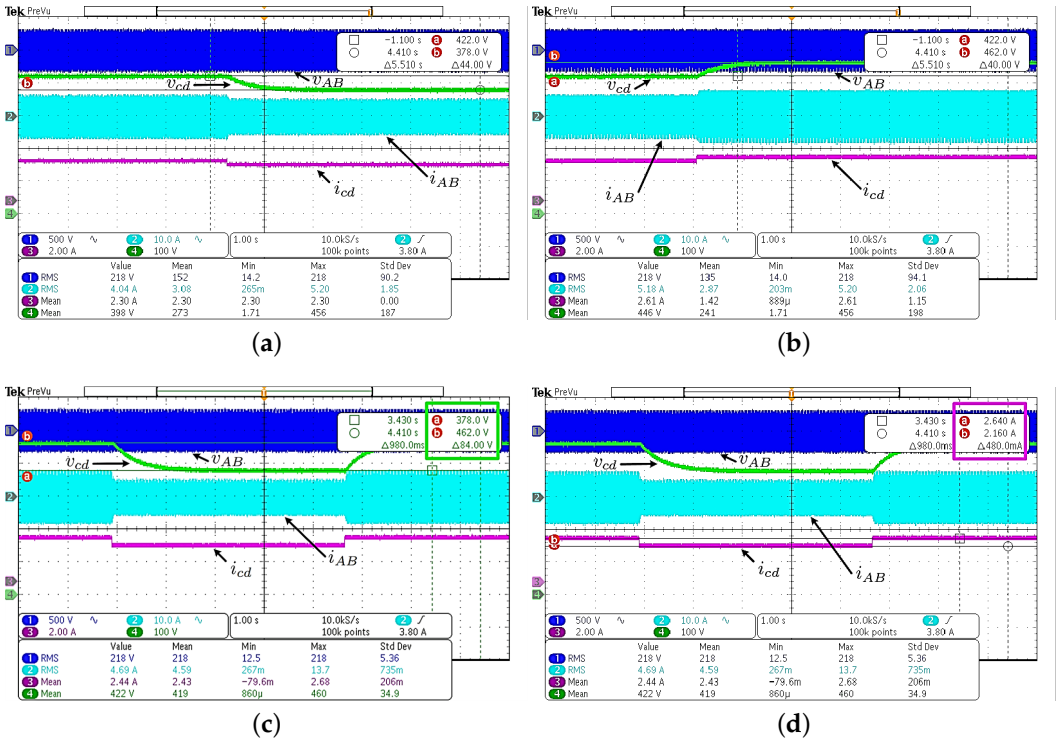

Figure 13. Performance of the PWM rectifier under DC voltage reference changes. (**a**) V_{dc} decreases −10%. (**b**) V_{dc} increases +10%. (**c**,**d**) V_{dc} changes from +10% to −10% and viceversa.

4.5. Harmonic Current Compensation

Another challenging test for the proposed control is by combining the function of the current filter and the PWM rectifier simultaneously. Figure 14 shows the PWM rectifier acting as a harmonic current compensator. At the beginning, the NLL is connected to the PCC but the rectifier follows only the fundamental component of the current reference as seen in Figure 14a,b; thus, the grid current supplies all the requirements of the NLL, resulting in a $\text{THD}_{iAB} = 18.74\%$. When the converter begins to compensate the harmonics of the NLL, the grid current continues providing the fundamental component but its THD decreases to 6.18% due to the active filter action. In order to not exceed the nominal power of the rectifier, for this test, the DC load increases to $1.2Z_L$ and, as a consequence, $P_{rect} = 0.833$ kW. According to this power, $\widetilde{i_{AB}} = 3.78\ \text{A}_{rms} = 5.35\ \text{A}_{peak}$, but by adding the load harmonics, its peak value increases until $\widetilde{i_{AB}} = 6.36$ A, as shown in Figure 14b. Also, due to the NLL demand, the grid current rises to $i_{AB} = 6.66\ \text{A}_{rms}$.

The harmonic content of currents i_{AB} and i_{nll} can be seen in Figure 14c and Figure 14d, respectively. The fundamental component of the NLL reaches $4\ \text{A}_{peak}$, and then the peak values of harmonics are obtained in agreement with (11). It can be observed from Figure 14b that the DC signals remain constant and that the current $i_{dc} = 2$ A, as a consequence of increasing Z_L to $211.68\ \Omega = 1.2 \times 176.4\ \Omega$.

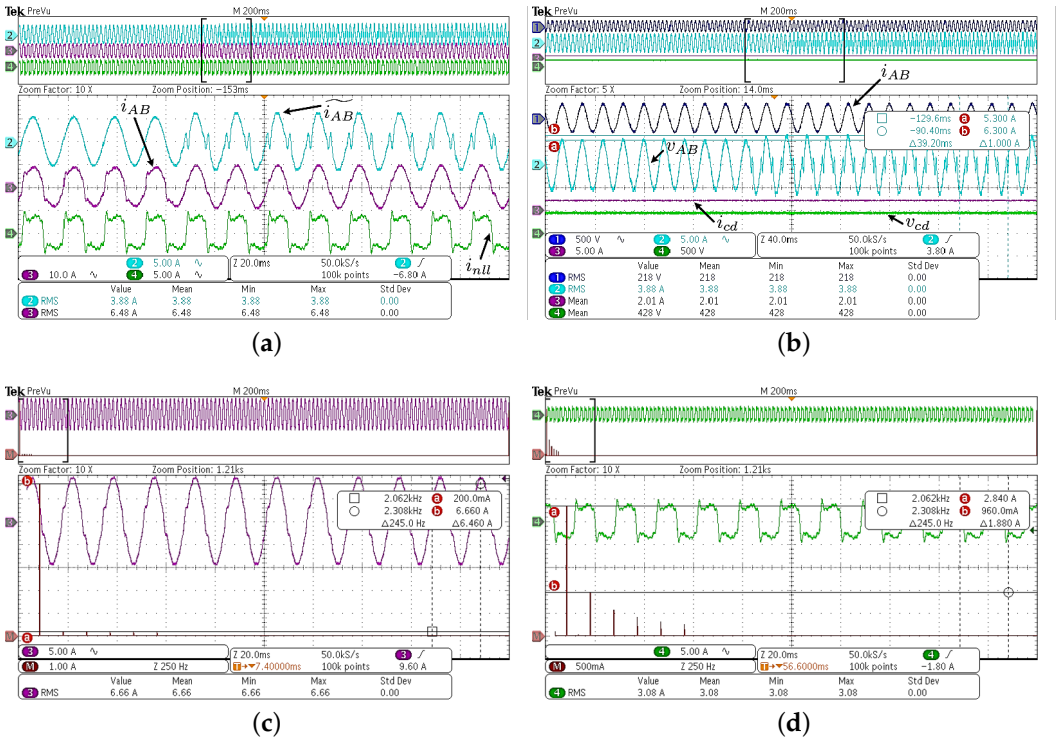

Figure 14. Performance of the PWM rectifier as an active current filter. (**a**) $\widetilde{i_{AB}}$, i_{AB} and i_{nll}. (**b**) v_{AB}, $\widetilde{i_{AB}}$, i_{dc} and v_{dc}. (**c**) Harmonic spectrum of i_{AB}. (**d**) Harmonic spectrum of i_{nll}.

4.6. Grid Voltage Sags, Dynamic DC Load and Harmonic Current Compensation Simultaneously

In Figure 15, the DC load changes and grid voltage sags occur while the rectifier compensates the current harmonics of the NLL. To assess a more severe scenario, as in previous subsections, the grid voltage decreases every 1 s, the DC load is modified with a frequency of 1 kHz, while the rectifier acts as an active filter. The grid voltage decreases by 25% and the DC load Z_L switches between 211.68 Ω and 270.48 Ω ($1.2Z_L + Z_L/3$). Consequently, the current i_{dc} changes from 2 A to 1.58 A and vice versa, as seen in Figure 15a. In order to maintain the power balance, when the grid voltage decreases, the current $\widetilde{i_{AB}}$ increases its peak value as shown in Figure 15b. Note that, even in the presence of these events, the PWM rectifier has a good performance.

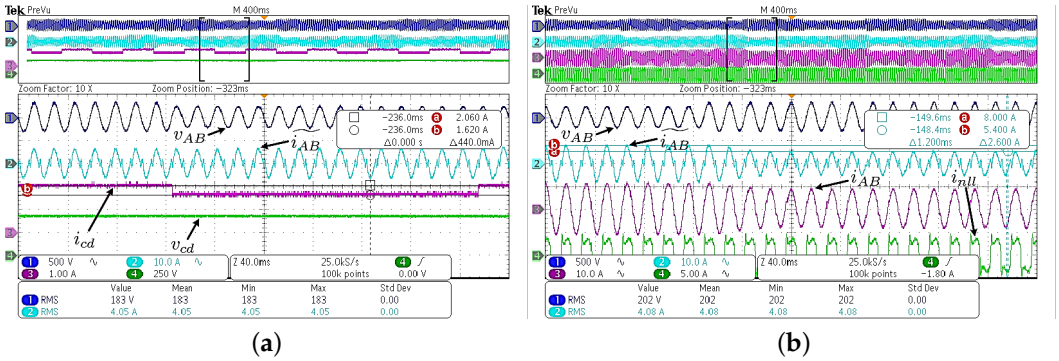

Figure 15. Performance of the PWM rectifier under grid voltage sags and load changes, acting as an active current filter simultaneously. (**a**) v_{AB}, $\widetilde{i_{AB}}$, i_{dc} and v_{dc}. (**b**) v_{AB}, $\widetilde{i_{AB}}$, i_{AB} and i_{nll}.

4.7. Grid Voltage Sags, Dynamic DC Load and Harmonic Current Compensation Simultaneously Considering a Grid Impedance

In order to evaluate a more realistic scenario, a grid impedance is added in series with the voltage source, as shown in Figure 16. The resistance and inductance values are proposed according to [24] as $R_g = 1.36\ \Omega$ and $L_g = 0.6$ mH. For $V_{AB} = 220\ V_{rms}$ and $|i_{AB}| = 3.78\ A_{rms}$, the voltage at the PCC is given by

$$|v_{pcc}| = V_{pcc} = V_{AB} - |i_{AB}|\,|R_g + i(120\pi L_g)| = 214.85\ V_{rms}. \tag{12}$$

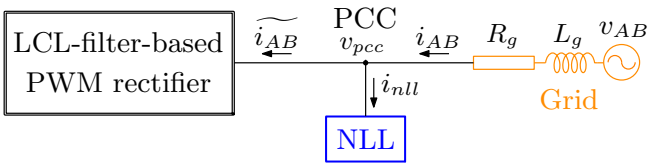

Figure 16. PWM rectifier representation using LCL filter, compensating the harmonic current of a nonlinear load connected at the PCC and considering a grid impedance.

Next, the behavior of the PWM rectifier at different operating points is evaluated.

In Figure 17a, the DC load changes while the rectifier compensates the current harmonics of the NLL. As can be seen in this figure, the grid voltage v_{AB} is not affected; thus, the magnitude of the voltage $V_{pcc} = 213\ V_{rms}$, which is very close to the value calculated in (12). The THD of the voltage at the PCC is 1.16%. Figure 17b shows the same operating point evaluated in Section 4.6: the DC load changes and grid voltage sags occur while the rectifier compensates the current harmonics of the NLL. Note that, by adding the grid impedance, the performance of the PWM rectifier is as close as in Figure 15.

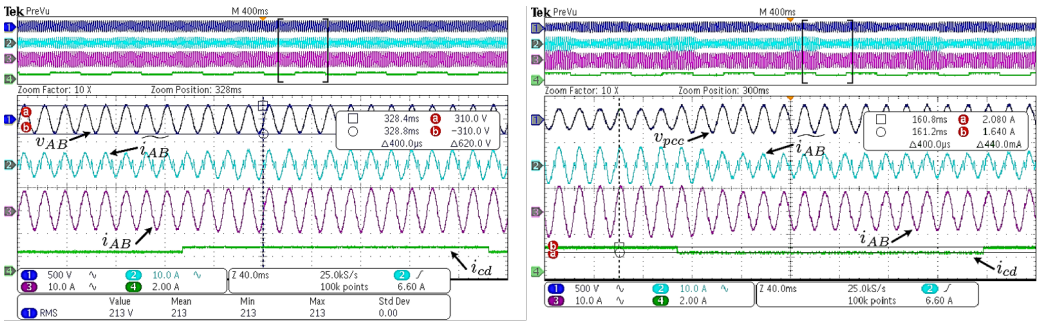

(**a**) (**b**)

Figure 17. Performance of the PWM rectifier under different scenarios and considering the grid impedance. (**a**) Under load changes, acting as an active current filter simultaneously. (**b**) Under voltage sags and load changes, acting as an active current filter simultaneously.

5. Conclusions

In this article, a concatenated approach for designing a PWM rectifier and tuning its control using the Butterworth polynomial synthesis is proposed. The approach is based on using the three linear equations of the LCL filter to control the entire fourth-order system, considering the assumptions explained in the article. Analytical developments and tests using the SIL approach have been carried out, which demonstrated that the PWM rectifier maintains its compensation and stability properties for regulating the DC bus, despite the reduction of the variables involved in the control. To test the PWM rectifier's performance under a complicated operational regime, multiple tests have been conducted, even performing tasks for which it was not designed. For instance, it can work simultaneously as a rectifier and an active filter, and it can manage voltage sags and dynamic loads in the rectifier mode. The results showed that no performance properties are lost when performing the Butterworth polynomial synthesis in both the design and control of the three-order system to control and operate the fourth-order system. It is worth noting

that the proposed approach does not require either making the control more complex with nonlinear controllers or using double control loops. Likewise, it is unnecessary to resort to *dq* transformations. The aforementioned factors contribute to the proposal appeal in the modern industrial electrical applications environment, where the need to control complex systems in a simple and robust manner is critical.

Author Contributions: Conceptualization, C.N., R.I.V.D. and N.V.C.; methodology, C.N., R.I.V.D. and N.V.C.; software, R.I.V.D.; validation, C.N. and R.I.V.D.; investigation, C.N. and R.I.V.D.; resources, N.V.C. and J.S.R.; writing, C.N. and R.I.V.D.; writing—review, N.V.C. and J.S.R. All authors have read and agreed to the published version of the manuscript.

Funding: This work was supported by Consejo Nacional de Humanidades Ciencia y Tecnología (CONAHCYT) under Project A1-S-29705 and by FORDECYT PRONACES/1311344.

Conflicts of Interest: The authors declare no conflict of interest. The funders had no role in the design of the study, in the collection, analyses, or interpretation of data, in the writing of the manuscript, or in the decision to publish the results.

References

1. Willis, C.H. Applications of Harmonic Commutation for Thyratron Inverters and Rectifiers. *Trans. Am. Inst. Electr. Eng.* **1933**, *52*, 701–707. [CrossRef]
2. Kakkar, S.; Maity, T.; Ahuja, R.K. Power quality improvement of PWM rectifier using VFOC and LCL filter. In Proceedings of the 2017 IEEE International Conference on Power, Control, Signals and Instrumentation Engineering (ICPCSI), Chennai, India, 21–22 September 2017 ; pp. 1036–1040. [CrossRef]
3. Deng, J.; Lei, Y.; Kang, J.S.; Yu, M. A Harmonic Current Suppression Method for Single-Phase PWM Rectifier Based on Feedback Linearization. In Proceedings of the International Conference on Power Energy Systems and Applications (ICoPESA), Singapore, 2022; pp. 90–95. [CrossRef]
4. Vaideeswaran, V.; Veerakumar, S.; Sharmeela, C.; Bharathiraja, M.; Chandrasekaran, P. Modelling of an Electric Vehicle Charging Station with PWM Rectifier to mitigate the Power Quality Issues. In Proceedings of the Transportation Electrification Conference (ITEC-India), New Delhi, India, 16–19 December 2021; pp. 1–6. [CrossRef]
5. Nunez, C.; Lira, J.; Visairo, N.; Echavarría, R. Analysis of the Boundaries to Compensate Voltage Sag Events Using a Single Phase Multi-Level Rectifier. *EPE J.* **2010**, *20*, 5–11. [CrossRef]
6. Tawfeeq, O.T.; Ibrahim, A.Y.; Alabbawi, A.A.M. Study of a Five-Level PWM Rectifier Fed DC Motor Drive. In Proceedings of the 7th International Conference on Electrical and Electronics Engineering (ICEEE), Antalya, Turkey, 14–16 April 2020; pp. 126–129. [CrossRef]
7. Changizian, M.; Mizani, A.; Shoulaie, A. A new frequency control method to enhance fault ride-through capability of VSC-HVDC systems supplying industrial plants. *Electr. Power Syst. Res.* **2023**, *214*, 108843. [CrossRef]
8. Yang, J.; Meng, N. Multi-loop power control strategy of current source PWM rectifier. *Energy Rep.* **2022**, *8*, 11675–11682. [CrossRef]
9. Bian, C.; Liu, S.; Xing, H.; Jia, Y. Research on fault-tolerant operation strategy of rectifier of square wave motor in wind power system. *CES Trans. Electr. Mach. Syst.* **2021**, *5*, 62–69. [CrossRef]
10. Lhachimi, H.; El Kouari, Y.; Sayouti, Y. Control strategy of DFIG for wind energy system in the grid connected mode. In Proceedings of the International Renewable and Sustainable Energy Conference (IRSEC), Marrakech, Morocco, 14–17 November 2016; pp. 515–520. [CrossRef]
11. Narayanan, V.; Kewat, S.; Singh, B. Solar PV-BES Based Microgrid System With Multifunctional VSC. *IEEE Trans. Ind. Appl.* **2020**, *56*, 2957–2967. [CrossRef]
12. Shwetha, G.; Guruswamy, K.P. Performance Analysis of PWM Rectifier as Charger for Electric Vehicle Application. In Proceedings of the International Conference on Integrated Circuits and Communication Systems (ICICACS), Raichur, India, 24–25 February 2023; pp. 1–7. [CrossRef]
13. Thangavel, S.; Mohanraj, D.; Girijaprasanna, T.; Raju, S.; Dhanamjayulu, C.; Muyeen, S.M. A Comprehensive Review on Electric Vehicle: Battery Management System, Charging Station, Traction Motors. *IEEE Access* **2023**, *11*, 20994–21019. [CrossRef]
14. Wai, R.J.; Yang, Y. Design of Backstepping Direct Power Control for Three-Phase PWM Rectifier. *IEEE Trans. Ind. Appl.* **2019**, *55*, 3160–3173. [CrossRef]
15. Verrelli, C.; Bigarelli, L.; di Benedetto, M.; Lidozzi, A.; Solero, L. A new nonlinear control of an active rectifier for variable speed generating units. *Control Eng. Pract.* **2023**, *139*, 105653. [CrossRef]
16. *Application Report: Understanding Boost Power Stages in Switchmode Power Supplies*; Technical Report; Texas Instrument: Dallas, TX, USA, 1999.
17. Sira-Ramirez, H.; Ortega, R.; Perez-Moreno, R.; Garcia-Esteban, M. A Sliding Controller-Observer for DC-to-DC Power Converters: A Passivity Approach. In Proceedings of the 1995 34th IEEE Conference on Decision and Control, New Orleans, LA, USA, 3–15 December 1995. [CrossRef]

18. Marzouki, A.; Hamouda, M.; Fnaiech, F. Nonlinear control of three-phase active rectifiers based L and LCL filters. In Proceedings of the International Conference on Electrical Engineering and Software Applications, Hammamet, Tunisia, 23–25 October 2013; pp. 1–5. [CrossRef]
19. Degioanni, F.; Zurbriggen, I.G.; Ordonez, M. Fast and Reliable Geometric-Based Controller for Three-Phase PWM Rectifiers. In Proceedings of the Applied Power Electronics Conference and Exposition (APEC), New Orleans, LA, USA, 15–19 March 2020; pp. 1891–1896. [CrossRef]
20. Foti, S.; Scelba, G.; Testa, A.; Sciacca, A. An Averaged-Value Model of an Asymmetrical Hybrid Multi-Level Rectifier. *Energies* **2019**, *12*, 589. [CrossRef]
21. Zverev, A.I. *Handbook of Filter Synthesis*; John Wiley and Sons, Inc.: Hoboken, NJ, USA, 1967.
22. Arellanes, A.; Nuñez, C.; Visairo, N.; Valdez-Fernandez, A.A. An Improvement of Holistic Control Tuning for Reducing Energy Consumption in Seamless Transitions for a BESS Grid-Connected Converter. *Energies* **2022**, *15*, 7964. [CrossRef]
23. *IEEE Std 1547-2018*; IEEE Standard for Interconnection and Interoperability of Distributed Energy Resources with Associated Electric Power Systems Interfaces. IEEE: New York, NY, USA, 2018.
24. Esparza, M.; Segundo, J.; Gurrola-Corral, C.; Visairo-Cruz, N.; Barcenas, E.; Barocio, E. Parameter Estimation of a Grid-Connected VSC Using the Extended Harmonic Domain. *IEEE Trans. Ind. Electron.* **2019**, *66*, 6044–6054. [CrossRef]